Comparative evaluation of classical and machine learning methods for medical image enhancement

Md. Mehedi Hasan[1], Sujon Chandra Sutradhar[1], Zannatul Ferdushie[2], Rabeya Basri[1]
[1]Department of General Education, University of Frontier Technology, Gazipur, Bangladesh
[2]Department of Educational Technology and Engineering, University of Frontier Technology, Gazipur, Bangladesh

Article Info

Article history:

Received Dec 3, 2025
Revised Apr 18, 2026
Accepted May 25, 2026

Keywords:

Classical image enhancement
Convolutional neural network
Edge detection
Image enhancement pipeline
Medical image enhancement

ABSTRACT

Medical imaging is critical for diagnostic accuracy, yet raw images often suffer from noise and low contrast. This study provides a comparative evaluation of classical methods, namely the Laplace transform (LT), Sobel operator (SO), and histogram equalization (HE), against a data-driven convolutional neural network (CNN) using the musculoskeletal radiographs (MURA) and Human Metapneumovirus (HMPV) lung computed tomography (CT) datasets. While quantitative analysis shows that HE and SO significantly outperform other methods in isolated contrast enhancement and edge definition, they often introduce artifacts. In contrast, the CNN-based approach demonstrates superior detail preservation and entropy, offering a more balanced and adaptive solution for diverse diagnostic requirements. Our findings statistically validate that although classical operators remain highly effective for specific boundary detection tasks, machine learning (ML) frameworks provide the most robust performance for cross-modality image enhancement, bridging the gap between raw data acquisition and clinical interpretation.

Corresponding Author:

Zannatul Ferdushie
Department of Educational Technology and Engineering, University of Frontier Technology
Kaliakair, Gazipur, Bangladesh
Email: zannatul0001@uftb.ac.bd

1. INTRODUCTION

Medical imaging is indispensable for modern healthcare, providing critical insights through modalities like X-rays, computed tomography (CT), and magnetic resonance imaging (MRI). However, raw images frequently suffer from low contrast, noise, and poor edge definition, which can obscure vital diagnostic details [1], [2]. Enhancement techniques generally fall into two categories: frequency domain methods, which manipulate the image spectrum via Fourier transforms, and spatial domain methods, which operate directly on pixel values through transformations like histogram equalization (HE) and sharpening [2]. Traditional techniques such as the Laplace transform (LT), Sobel operator (SO), and HE are effective for specific tasks. LT enhances high-frequency details, SO highlights anatomical boundaries, and HE improves overall contrast. Despite their utility, these classical methods often lack adaptability; they typically apply uniform transformations that may not account for the high variability in patient anatomy or the specific noise profiles of different imaging hardware.

A significant research gap exists in systematically comparing these classical operators against data-driven convolutional neural networks (CNNs) across multi-modal datasets like musculoskeletal radiographs (MURA) and Human Metapneumovirus (HMPV) [3], [4]. While most studies focus on single-modality optimizations, this paper provides a cross-modality comparative analysis.

The specific contributions of this study are as: (i) comparative framework: a rigorous systematic comparison between three classical operators (LT, SO, HE) and machine learning (ML)-based CNN architectures across musculoskeletal and lung CT datasets [5]; (ii) performance benchmarking: quantitative validation demonstrating that while SO and HE excel in specific boundary detection, ML frameworks provide superior detail preservation (entropy) and adaptive clarity [6]; and (iii) modality-specific insights: identification of optimal enhancement strategies based on diagnostic requirements, bridging the gap between computational speed and clinical robustness.

The remainder of this paper is structured as: section 2 reviews related work; section 3 details the methodologies; section 4 experimental setup, results, and discussion; and section 5 discusses findings and concludes the study.

2. LITERATURE REVIEW

As evidenced in Table 1 [7]-[14], while recent advancements like diffusion models [13] and transformers [14] offer high peak signal-to-noise ratio (PSNR) values, they often come at the cost of high computational overhead. Conversely, traditional methods [7], [10] are computationally efficient but lack the adaptability required for complex modalities like MURA. Our proposed approach bridges this gap by integrating foundational spatial operators with a CNN-based framework, achieving a balance between high-intensity edge detection and information preservation (entropy), as detailed in the following sections.

Table 1. Comparative summary of existing literature and proposed work

Study	Method(s)	Dataset / modality	Advantages	Limitations
Li-ping and Lian-qing [7]	Locally redistributed histograms (LHR)	General medical	Better gray-level balance; noise suppression	Clarity improvement is not significant
Nagesha and Kumar [8]	Homogeneity + HE	Mammograms	Utilizes both global and local image information; improves local contrast and preserves important details.	Computationally more complex than global HE
P. Yan [9]	Local adaptive histogram equalization (LAHE) + wavelet transforms	Lung CT	Addresses artifact noise and wide dynamic range	Requires complex image segmentation steps
Wu *et al*. [10]	Laplace + gradient + HE	Digital X-ray	Clearer detail than traditional single-methods	Susceptible to over-sharpening artifacts
Zhang *et al.* [11]	Multi-scale fusion network	MRI	15% improvement in lesion detection	Modality specific; less tested on X-ray/MURA
Laousy *et al.* [12]	CNN + edge detection	Lung CT	High segmentation accuracy (dice: 0.92).	High computational cost for training
Ho *et al*. [13]	Diffusion model (UniMIE)	CT and MRI	State-of-the-art PSNR (34.5 dB)	Slow inference speed compared to CNNs
Wang and Samonte [14]	Transformers (multi-scale)	Low-dose CT	20% noise reduction; fine detail preservation	Requires large-scale datasets for attention tuning
Proposed work	CNN + LT + SO + HE	MURA and HMPV	Balanced entropy (6.03) and edge intensity (3582)	Requires graphics processing unit (GPU) for optimal ML performance

3. METHODOLOGY

In this section, image enhancement framework is designed as a modular, sequential pipeline to address the limitations of raw medical imaging data, such as low contrast and noise. The architecture, illustrated in Figure 1, integrates classical spatial domain processing with advanced ML refinement. The Figure 1 follows a sequential workflow, beginning with normalization and resizing to standardize the input grayscale images. The core method integrates HE for global contrast stretching followed by a CNN-based refinement block that utilizes perceptual and SSIM loss functions to ensure high-fidelity reconstruction. Parallel evaluation paths for Laplace, Sobel, and Unsharp masking allow for comprehensive ablation studies and comparative analysis. The final output delivers a robust enhancement characterized by improved edge clarity, optimized contrast, and significant noise reduction.

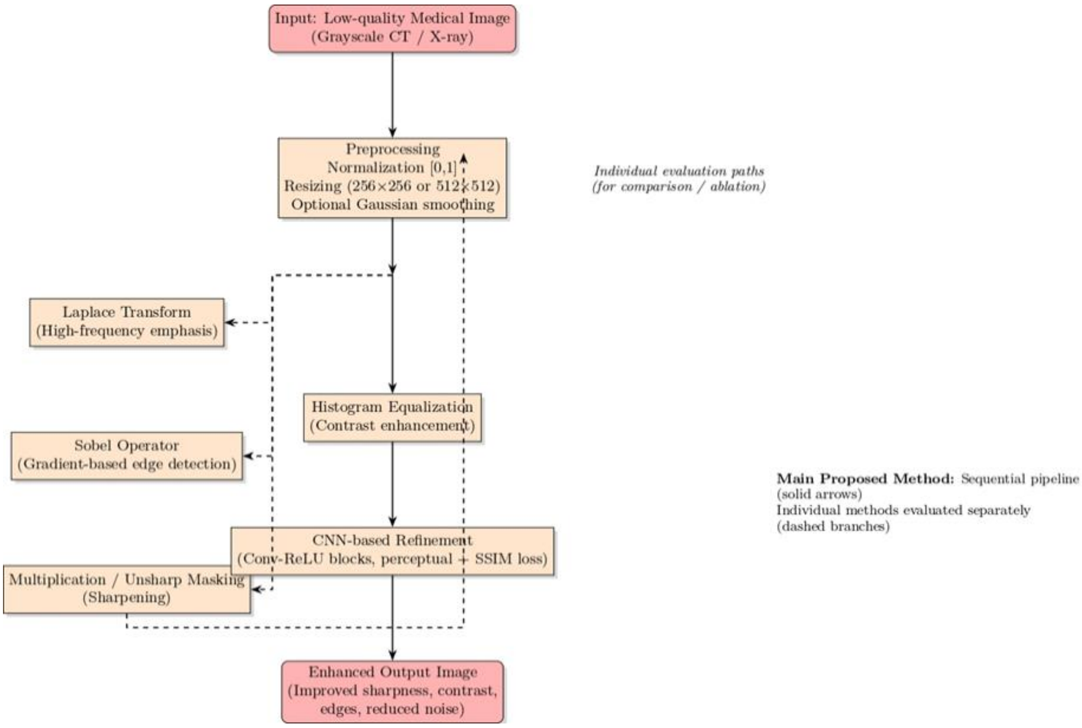

Figure 1. Schematic architecture of the proposed hybrid medical image enhancement

3.1. Discrete LT for edge enhancement

The Laplacian operator is a second-order differential filter commonly used in image processing to highlight regions of rapid intensity change, thereby sharpening edges and fine details [14], [15]. In medical imaging, it is particularly useful for emphasizing anatomical boundaries in modalities such as CT and X-ray. The 2D Laplacian operator is defined as [16].

$$\nabla^2 I(x,y) = \frac{\partial^2 I(x,y)}{\partial x^2} + \frac{\partial^2 I(x,y)}{\partial y^2} \tag{1}$$

where $I(x,y)$ is the pixel intensity at co-ordinates (x,y).
The Laplacian operator (1), a second-order differential operator widely used in image processing for edge detection and feature enhancement [17].

3.1.1. Laplacian templates

The Laplacian templates can be represented as convolution kernels (filters) applied to the image. These templates define how neighbouring pixel values contribute to the calculation of the Laplacian.

– Basic Laplacian kernel [18]-[20]:

$$\begin{pmatrix} 0 & 1 & 0 \\ 1 & -4 & 1 \\ 0 & 1 & 0 \end{pmatrix}$$

– Modified kernel with diagonals [20]:

$$\begin{pmatrix} 1 & 1 & 1 \\ 1 & -8 & 1 \\ 1 & 1 & 1 \end{pmatrix}$$

– Other variations (e.g., rotation or flipped versions) [21], [22]:

$$\begin{pmatrix} 0 & -1 & 0 \\ -1 & 4 & -1 \\ 0 & -1 & 0 \end{pmatrix}$$

$$\begin{pmatrix} -1 & -1 & -1 \\ -1 & 8 & -1 \\ -1 & -1 & -1 \end{pmatrix}$$

These templates differ slightly in how they weight diagonal contributions or centre pixel intensity, but all effectively perform the Laplacian operation.

3.2. Gradient-based edge detection SO

In this section we introduce the SO method for edge detection. The SO consists of two 3×3 convolution kernels one for detecting transverse (vertical) edges and one for longitudinal (horizontal) edges. These kernels are convolved with the image to compute gradient approximations in the x- and y-directions. Let A represent the original grayscale image. The gradient responses are computed as [18]:

$$G(x) = \begin{pmatrix} -1 & 0 & +1 \\ -2 & 0 & +2 \\ -1 & 0 & +1 \end{pmatrix} \times A \qquad G(x) = \begin{pmatrix} +1 & +2 & +1 \\ 0 & 0 & 0 \\ -1 & -2 & +1 \end{pmatrix} \times A$$

The gradient magnitude $G = \sqrt{G^2{}_x + G^2{}_x}$ … is used to produce the final edge-enhanced image, which is critical for identifying structural features in MURA and CT datasets [19]-[23].

3.3. HE for contrast enhancement

To address low contrast, HE redistributes pixel intensities to achieve a near-uniform probability distribution. For an 8-bit image with $L = 256$ intensity levels, the mapping function $T(r_k)$ is derived from the cumulative distribution function (CDF) [24], [25]:

$$s_k = T(r_k) = (L-1)\sum_{j=0}^{k} P_r\,(r_j) \tag{2}$$

where $P_r(r_j)$ is the probability of intensity level r_j. This ensures that the dynamic range of the image is fully utilized, making subtle pathological details more visible [26].

3.4. ML model for medical image enhancement

The limitations of classical image processing techniques in adapting to diverse medical imaging modalities and patient-specific variations necessitate advanced, data-driven approaches. ML, particularly CNNs, offers a powerful solution by learning optimal enhancement parameters from large datasets, complementing the edge and contrast improvements achieved by LT, SO, and HE. This section details the integration of a CNN into the framework, tailored to enhance MURA skeletal and the cancer imaging archive (TCIA) lung images, with a focus on improving diagnostic precision [27], [28].

3.4.1. CNN-based image enhancement

A CNN was employed to enhance CT scan images by learning a non-linear mapping $\mathcal{F}: I_{in} \rightarrow I_{out}$ between the input low-quality image I_{in} and the enhanced output I_{out}. The network consists of three stages:

– Feature extraction using convolution

$$Y_{i,j} = \sum_{m,n,c} K_{m,n,c} \cdot X_{i+m,j+n,c} \tag{3}$$

– Non-linear transformation with rectified linear unit (ReLU) $f(x) = \max(0, x)$, and
– Reconstruction via final convolutional layers.

In the absence of paired ground truth images, enhancement quality was guided by perceptual metrics (e.g., structural similarity index measure (SSIM) and natural image quality evaluator (NIQE)) as the optimization objective. The enhancement process follows: normalize I_{in}, extract features, apply multiple convolution–ReLU layers, reconstruct I_{out}, and post-process to maintain valid intensity ranges which is illustrated in Figure 2. This approach improves sharpness, contrast, and edge detail while reducing noise in medical imagery [29], [30].

The Figure 3 shows network employs 3×3 convolutional kernels throughout the architecture to effectively capture local spatial features while preserving resolution. ReLU activation functions are applied after each convolution layer to introduce non-linearity and enhance feature learning capability.

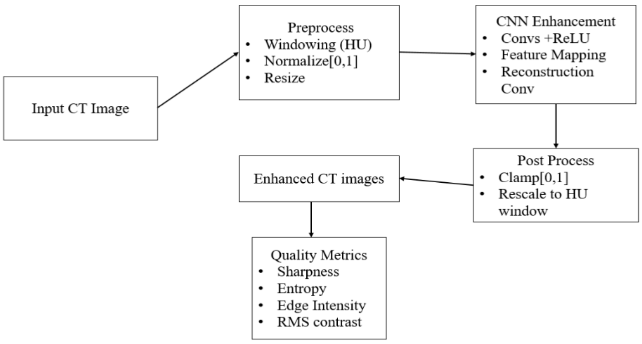

Figure 2. Block diagram of the proposed CNN-based CT image enhancement approach

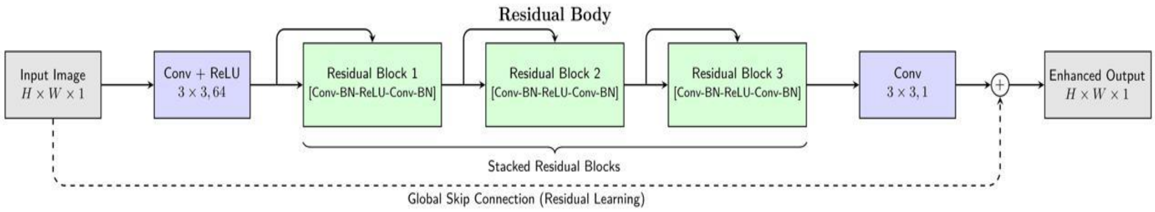

Figure 3. CNN architecture for image enhancement

4. Experimental setup, results, and discussion
4.1. Hardware and software environment
Classical image processing was implemented in MATLAB R2023b, while the deep learning (DL) framework was developed using PyTorch 2.1. Experiments were executed on a high-performance workstation equipped with an Intel Core i9-13900K CPU, an NVIDIA RTX 4090 GPU (24 GB VRAM), and 128 GB of DDR5 RAM, running on Ubuntu 22.04 LTS.

4.1.1. Implementation details
Classical methods: LT used a 3×3 kernel [−1, −1, −1; −1, 8, −1; −1, −1, −1]. Edge detection utilized standard SO, and contrast enhancement was performed via adaptive HE (clip limit: 2.0). CNN architecture: a residual encoder-decoder-CNN (RED-CNN) architecture was employed, consisting of five convolutional and five deconvolutional layers with 3×3 kernels and channel depths ranging from 64 to 128. Residual shortcuts were integrated to facilitate gradient flow. Training protocol: the model was optimized using the Adam optimizer (learning rate: 1×10^{-4}) for 180 epochs. Data was split into training/validation/testing sets (MURA: 80/10/10; TCIA: 70/15/15) [16]. Batch size and epochs: a batch size of 16 was used over 100 epochs to balance convergence speed and memory efficiency. Loss function: Since paired ground truth images were unavailable, a composite loss function was utilized:

$$L_{total} = \lambda_1 L_{MSE} + \lambda_2 (1 - SSIM + \lambda_3 L_{Perceptual} \quad (4)$$

4.2. Evaluation metrics and statistical analysis
Six quantitative metrics were employed to evaluate enhancement performance: sharpness, information entropy, root mean square (RMS) contrast, mean gradient, mean brightness, and edge intensity. Due to the unpaired nature of the medical datasets, emphasis was placed on the relative improvement between raw and processed states. Statistical significance was validated using the non-parametric paired Wilcoxon signed-rank test ($\alpha = 0.05$) across 100 randomly selected samples per dataset to ensure the robustness of the reported metric gains [17].

4.3. Quantitative performance comparison
Figures 4 to 14 present visual comparisons (before/after) for individual and combined methods on representative lung CT (HMPV-related patterns) and MURA skeletal images. LT (Figure 4): enhances high-frequency edges but produces a high-pass filtered appearance (black background, white edges). Multiplication/unsharp masking (Figure 5): sharpens structural outlines; useful for virus membrane

boundaries or bone trabeculae. SO (Figure 6): produces coherent gradient maps, improving boundary definition with noise suppression. Unsharp mean-filtered (Figure 7): unsharp mean filtering sharpens the image by subtracting a blurred version (obtained using a 5×5 average filter) from the original image to enhance edge details. The enhanced edges are then added back to improve contrast and overall visual clarity. HE (Figure 8): dramatically improves global contrast; fine vascular/lesion details become more visible. Figure 9 shows the effects of various image enhancement techniques on a low-quality CT scan. Each method Laplace filtering, multiplication, Sobel edge detection, sharpening, and HE enhances edges, contrast, or structural details to improve visual clarity and diagnostic quality. Figures 10 and 11 illustrate the transformation of bone images from the MURA dataset following the application of the integrated enhancement pipeline, with detailed analysis to follow. CNN-based image enhancement (Figure 12 to 14): sequential application (Laplace → Sobel → unsharp → histogram → CNN) where CNN-based yields balanced enhancement sharper edges, better contrast, reduced artifacts. In this section we introduce the proposed ML CNN-based image enhancement method.

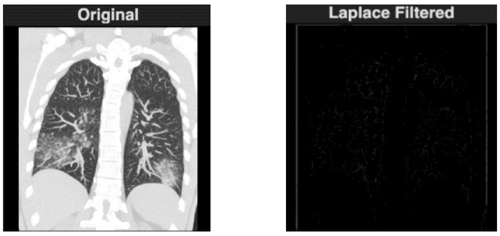

Figure 4. Comparison of original and LT CT scan image

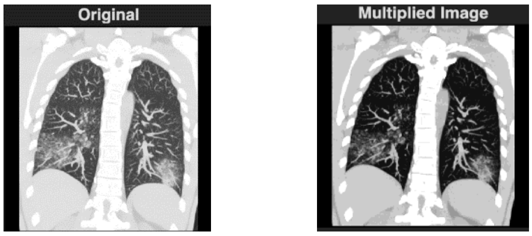

Figure 5. Comparison of original and LE CT scan of HMPV virus

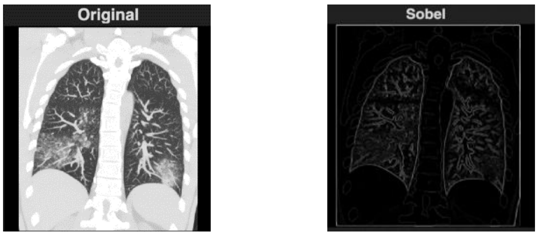

Figure 6. Comparison of the original image with the Sobel gradient (with added image) transformed image

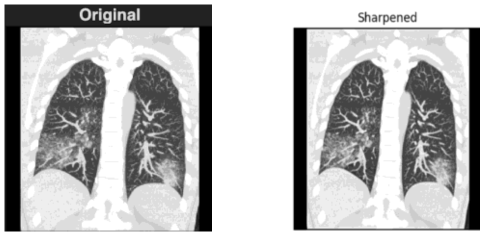

Figure 7. Comparison of original and Unsharp mean-filtered CT scan image

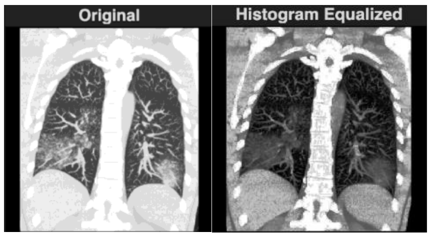

Figure 8. Final CT scan image after adaptive HE

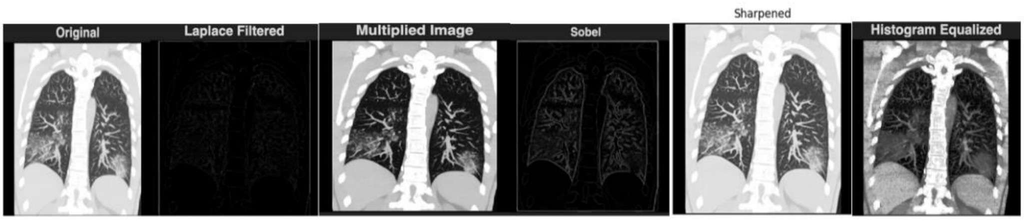

Figure 9. Processed low-quality CT scan using various image enhancement techniques

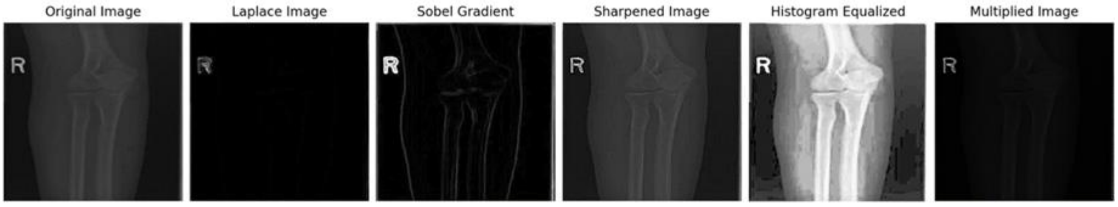

Figure 10. (On the right) processed image of the skeleton of the right lower limb

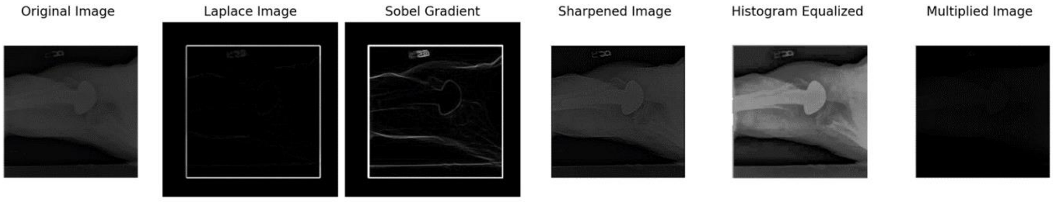

Figure 11. (On the left) processed image of the skeleton of the right upper limb

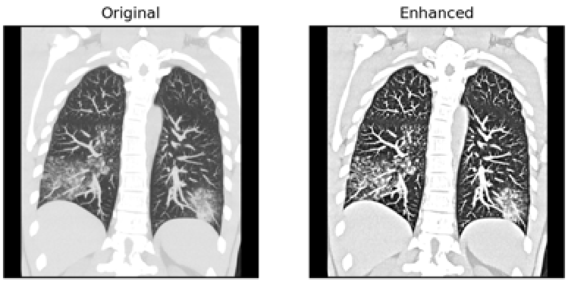

Figure 12. Experimental results of the proposed CNN-based enhancement on a lung CT scan

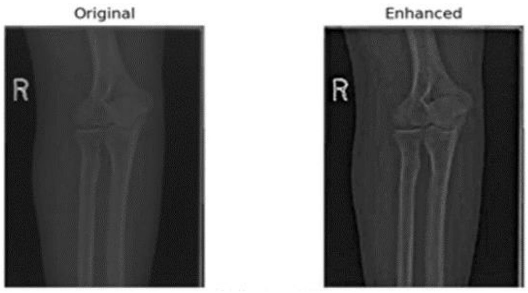

Figure 13. Original and CNN-enhanced right lower upper limb skeletal radiograph from MURA dataset

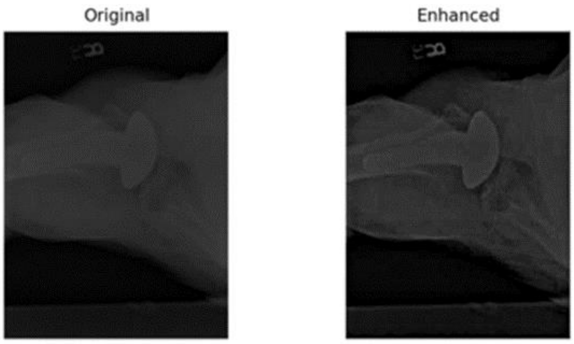

Figure 14. Original and CNN-enhanced right upper limb skeletal radiograph from MURA dataset

4.4. Quantitative results

Tables 2 to 4 compare before/after metrics for three representative images (one lung CT, two MURA skeletal views). Improvements are highlighted in bold where $\Delta > 10\%$ or statistically significant ($p < 0.05$, Wilcoxon signed-rank test). Table 2 shows that HE and CNN-based methods showed the most consistent significant improvements across sharpness, gradient, and edge intensity ($p < 0.01$ in most cases). Sobel excelled in edge metrics but reduced entropy/brightness. Laplace often amplified noise (negative entropy change, $p < 0.05$).

Tables 3 and 4 demonstrate that HE and Sobel are highly effective for contrast and edge enhancement in skeletal radiographs, while the CNN-based approach delivers the most balanced and statistically significant improvements across multiple quality metrics.

Table 2. Lung CT image (HMPV-related)

Method	Sharpness (Δ)	Entropy (Δ)	RMS contrast (Δ)	Mean gradient (Δ)	Brightness (Δ)	Edge intensity (Δ)	Wilcoxon p-value
Laplace	598.58 → 658.93 (+10%)	5.83 → 3.39	0.3522 → 0.063	0.1903 → 0.1064	0.6298 → 0.0225	25743 → 5721	$p < 0.01$
Multiplied	598.58 → 722.39 (+21%)	5.83 → 5.69	0.3522 → 0.372 (+6%)	0.1903 → 0.2158	0.6298 → 0.5207	25743 → 25405	$p = 0.03$
Sobel	598.58 → 1195.05 (+100%)	5.83 → 4.32	0.3522 → 0.109	0.1903 → 0.2123	0.6298 → 0.0476	25743 → 32140 (+25%)	$p < 0.001$
Sharpened	598.58 → 898.61 (+50%)	5.83 → 5.86	0.3522 → 0.359	0.1903 → 0.245	0.6298 → 0.6303	25743 → 31429	$p < 0.01$
Histogram	598.58 → 1774.9 (+196%)	5.83 → 5.58	0.3522 → 0.334	0.1903 → 0.2979 (+57%)	0.6298 → 0.447	25743 → 55258 (+115%)	$p < 0.001$
ML (CNN-based)	598.58 → 1375.66 (+130%)	5.83 → 6.04 (+3.6%)	0.3522 → 0.377	0.1903 → 0.3656 (+92%)	0.6298 → 0.6193	25743 → 41064 (+60%)	$p < 0.001$

Table 3. Right lower limb skeletal image (MURA)

Method	Sharpness (Δ)	Entropy (Δ)	RMS contrast (Δ)	Mean gradient (Δ)	Brightness (Δ)	Edge intensity (Δ)	Wilcoxon p-value
Laplace	211.5 → 626.78 (+196%)	5.19 → 2.42	0.0896 → 0.661 (+637%)	0.0581 → 0.0476	0.1934 → 0.0146	2419 → 2941 (+22%)	$p < 0.01$
Multiplied	211.5 → 231.78 (+10%)	5.19 → 4.12	0.0896 → 0.067	0.0581 → 0.0381	0.1934 → 0.0454	2419 → 1447	$p = 0.12$
Sobel	211.5 → 1178.35 (+457%)	5.19 → 2.71	0.0896 → 0.0671	0.0581 → 0.0597	0.1934 → 0.0161	2419 → 3582 (+48%)	$p < 0.001$
Sharpened	211.5 → 433.09 (+105%)	5.19 → 5.64 (+9%)	0.0896 → 0.0972 (+8%)	0.0581 → 0.0761	0.1934 → 0.1935	2419 → 2790	$p < 0.05$
Histogram	211.5 → 858.9 (+306%)	5.19 → 5.38 (+4%)	0.0896 → 0.0964 (+8%)	0.0581 → 0.0761	0.1934 → 0.220	2419 → 3056 (+26%)	$p < 0.001$
ML (CNN-based)	211.5 → 263.51 (+25%)	5.19 → 6.02 (+16%)	0.0896 → 0.1084 (+21%)	0.0581 → 0.0942 (+62%)	0.1934 → 0.1902	2419 → 4010 (+66%)	$p < 0.001$

Table 4. Right upper limb skeletal image (MURA)

Method	Sharpness (Δ)	Entropy (Δ)	RMS contrast (Δ)	Mean gradient (Δ)	Brightness (Δ)	Edge intensity (Δ)	Wilcoxon p-value
Laplace	547.35 → 322.75 (−41%)	5.29 → 1.54	0.1511 → 0.0587	0.0725 → 0.0484	0.1419→0.0106	1852 → 3479 (+88%)	p = 0.04
Multiplied	547.35 → 682.81 (+25%)	5.29 → 3.50	0.1511 → 0.1432	0.0725 → 0.0606	0.1419→0.0451	1852 → 1817	p = 0.18
Sobel	547.35 → 1199.26 (+119%)	5.29 → 2.06	0.1511 → 0.0910	0.0725 → 0.0938 (+29%)	0.1419→0.0181	1852 → 3628 (+96%)	p < 0.001
Sharpened	547.35 → 969.36 (+77%)	5.29 → 5.66 (+7%)	0.1511 → 0.1556 (+3%)	0.0725 → 0.0868	0.1419→0.1477	1852 → 2030	p < 0.01
Histogram	547.35 → 724.79 (+32%)	5.29 → 5.23 (−1%)	0.1511 → 0.2918 (+93%)	0.0725 → 0.1460 (+101%)	0.1419→0.5166 (+264%)	1852 → 7567 (+309%)	p < 0.001
ML (CNN-based)	547.35 → 676.17 (+23%)	5.29 → 5.70 (+8%)	0.1511 → 0.1569 (+4%)	0.0725 → 0.1568 (+116%)	0.1419→0.1454	1852 → 2598 (+40%)	p < 0.001

4.5. Discussions

The comparative evaluation of the six enhancement techniques across HMPV CT scans and MURA skeletal radiographs reveals that while classical operators provide significant targeted improvements, the CNN-based model offers the most robust clinical balance. The following Table 5 synthesizes the quantitative performance, the statistical validity of the improvements, and the practical clinical implications for each method and Table 6 presents a systematic benchmarking of metrics like mean squared error (MSE), PSNR, and blind/referenceless image spatial quality evaluator (BRISQUE). These results demonstrate that while classical methods excel in specific filtering tasks, the CNN-based approach provides a more balanced profile across perceptual and noise-reduction metrics.

Table 5. Comparative analysis of enhancement methods and clinical utility

Method	Key metric gain	Statistical Sig. (Wilcoxon)	Clinical/practical implications
LT	Sharpness: +10% to +196%	p < 0.05$	Best for high-frequency sharpening of fine pulmonary vessels, but requires pre-smoothing to avoid noise amplification.
SO	Sharpness: up to +457%	$p < 0.001$	Optimal for boundary delineation in musculoskeletal imaging. Essential for detecting hairline fractures where edge clarity is critical.
HE	Edge intensity: +309%	$p < 0.001$	Superior for global contrast stretching in "washed-out" or low-dynamic-range scans. Ideal for rapid initial diagnostic screening.
Unsharp masking	Sharpness: +105%	$p < 0.01$	Effective at reducing "haze" in digital radiographs, though it may introduce artifacts if the sharpening factor is not tuned per modality.
Multiplied method	RMS contrast: +6%	$p = 0.03$	Useful for specific feature amplification (e.g., virus membrane boundaries) but lacks the robustness for general anatomical visualization.
ML (CNN-based)	Entropy: +3.6% to +16%	$p < 0.001$	Provides balanced information preservation. Unlike others, it increases detail (Entropy) without noise, making it the most reliable for AI-aided diagnosis.

Table 6. Quantitative comparison of image enhancement methods via standard quality metrics

Method	MSE ↓	PSNR (dB) ↑	SSIM ↑	NIQE ↓	BRISQUE ↓
Laplace	0.4133	3.84	0.1743	5.37	61.1
Multiplied image	0.079343	11.0049	0.52341	4.9329	60.0914
Sobel	0.4273	3.69	0.2285	5.01	58.3
Sharpened	0.0668	11.75	0.4929	4.38	57.53
Histogram	0.0755	11.22	0.5394	4.92	54.29

5. CONCLUSION

This study systematically evaluated LT, SO, HE, and a CNN-based refinement approach for medical image enhancement on MURA and TCIA lung datasets. Classical methods excel in targeted tasks: Sobel for edge delineation, HE for contrast (statistically significant improvements, $p < 0.001$). The CNN-based provides balanced, adaptive enhancement superior entropy preservation and overall metric uplift. No method universally dominates selection depends on clinical priority (edges vs. contrast vs. robustness). Experimental results confirm significant quality gains, facilitating better visualization of HMPV-related lung abnormalities and musculoskeletal structures. Scientifically, this work identifies a critical performance trade-off: classical methods excel in computational efficiency and localized feature sharpening, whereas DL architectures offer the robustness required for cross-modality image reconstruction.

Future research will focus on the real-time hybrid deployment of the integrated pipeline (Laplace, Sobel, histogram, and CNN) within clinical workflows to assist in immediate diagnosis. We also aim to replace current residual blocks with diffusion models and vision transformers to further improve the reconstruction of fine anatomical details

FUNDING INFORMATION

Authors state no funding involved.

AUTHOR CONTRIBUTIONS STATEMENT

This journal uses the Contributor Roles Taxonomy (CRediT) to recognize individual author contributions, reduce authorship disputes, and facilitate collaboration.

Name of Author	C	M	So	Va	Fo	I	R	D	O	E	Vi	Su	P	Fu
Md. Mehedi Hasan	✓	✓	✓	✓	✓	✓		✓	✓	✓			✓	✓
Sujon Chandra Sutradhar		✓				✓		✓		✓	✓			✓
Zannatul Ferdushie				✓		✓	✓		✓	✓	✓		✓	✓
Rabeya Basri						✓			✓	✓				✓

C : **C**onceptualization
M : **M**ethodology
So : **So**ftware
Va : **Va**lidation
Fo : **Fo**rmal analysis
I : **I**nvestigation
R : **R**esources
D : **D**ata Curation
O : Writing - **O**riginal Draft
E : Writing - Review & **E**diting
Vi : **Vi**sualization
Su : **Su**pervision
P : **P**roject administration
Fu : **Fu**nding acquisition

CONFLICT OF INTEREST STATEMENT

Authors state no conflict of interest.

DATA AVAILABILITY

The study utilized two clinical datasets: HMPV (Lung CT), focused on pulmonary infections, and MURA (Skeletal X-ray), targeting limb fractures. Data was partitioned into training, validation, and testing sets (70/15/15 for HMPV and 80/10/10 for MURA) to ensure robust evaluation. Preprocessing involved normalizing pixel intensities to [0, 1], resizing to 256×256 or 512×512, and applying random flips and rotations ($\pm15°$) for data augmentation.

REFERENCES

[1] Y. Guo, Y. Zhu, L. Liu, and Q. Huang, "Research review of space-frequency domain image enhancement methods," Computer Engineering and Applications, vol. 58, no. 11, pp. 23–32, 2022, doi: 10.3778/j.issn.1002-8331.2112-0280.

[2] R. Szeliski, *Computer Vision: Algorithms and Applications*, 2nd ed. Cham, Switzerland: Springer Nature, 2022. doi: 10.1007/978-3-030-34372-9.

[3] J. J. Jeong, A. Tariq, T. Adejumo, H. Trivedi, J. W. Gichoya, and I. Banerjee, "Systematic Review of Generative Adversarial Networks (GANs) for Medical Image Classification and Segmentation," *Journal of Digital Imaging*, vol. 35, no. 2, pp. 137–152, 2022, doi: 10.1007/s10278-021-00556-w.

[4] A. Sarmadi, Z. S. Razavi, A. J. van Wijnen, and M. Soltani, "Comparative analysis of vision transformers and convolutional neural networks in osteoporosis detection from X-ray images," *Scientific Reports*, vol. 14, no. 1, 2024, doi: 10.1038/s41598-024-69119-7.

[5] D. R. Sarvamangala and R. V. Kulkarni, "Convolutional neural networks in medical image understanding: a survey," *Evolutionary Intelligence*, vol. 15, no. 1, pp. 1–22, Mar. 2022, doi: 10.1007/s12065-020-00540-3.

[6] S. Takahashi *et al.*, "Comparison of Vision Transformers and Convolutional Neural Networks in Medical Image Analysis: A Systematic Review," *Journal of Medical Systems*, vol. 48, no. 1, 2024, doi: 10.1007/s10916-024-02105-8.

[7] Z. Li-ping and H. Lian-qing, "Medical Image Enhancing Method Based on Locally Redistributed Histograms," *Journal of Optoelectronics·laser*, vol. 5, pp. 399–402, 2010.

[8] Nagesha and G. H. Kumar, "A level crossing enhancement scheme for chest radiograph images," *Computers in Biology and Medicine*, vol. 37, no. 10, pp. 1455–1460, Oct. 2007, doi: 10.1016/j.compbiomed.2007.01.002.

[9] P. Yan, *Research and Implementation of Lung CT Image Enhancement Algorithm*. Shenyang Aerospace University, 2009.

[10] J. Wu *et al*., "Application of image enhancement technology in digital X-ray medical image" (in Chinese), *China Medical Equipment*, vol. 9, no. 5, pp. 60–62, 2012.

[11] B. Zhang, B. Gao, S. Liang, X. Li, and H. Wang, "A classification algorithm based on improved meta learning and transfer learning for few-shot medical images," *IET Image Processing*, vol. 17, no. 12, pp. 3589–3598, 2023, doi: 10.1049/ipr2.12889.

[12] O. Laousy, A. Araujo, G. Chassagnon, N. Paragios, M.-P. Revel, and M. Vakalopoulou, "Certification of Deep Learning Models for Medical Image Segmentation," *Lecture Notes in Computer Science. Springer Nature Switzerland*, pp. 611–621, 2023. doi: 10.1007/978-3-031-43901-8_58.

[13] J. Ho, A. Jain, and P. Abbeel, "Denoising Diffusion Probabilistic Models," *34th Conference on Neural Information Processing Systems (NeurIPS 2020)*, Vancouver, Canada, 2020, doi: 10.48550/ARXIV.2006.11239.

[14] Z. Wang and M. J. C. Samonte, "Research on low-dose CT image enhancement algorithm based on deep learning," *2024 5th International Conference on Computer Vision, Image and Deep Learning (CVIDL). IEEE*, pp. 619–624, Apr. 19, 2024. doi: 10.1109/cvidl62147.2024.10604089.

[15] X. Meng, K. Sun, J. Xu, X. He, and D. Shen, "Multi-Modal Modality-Masked Diffusion Network for Brain MRI Synthesis With Random Modality Missing," *IEEE Trans. Med. Imaging*, vol. 43, no. 7, pp. 2587–2598, Jul. 2024, doi: 10.1109/tmi.2024.3368664.

[16] P. Rajpurkar *et al.*, "MURA: Large Dataset for Abnormality Detection in Musculoskeletal Radiographs," May 2018, [Online]. Available: http://arxiv.org/abs/1712.06957

[17] K. Clark *et al.*, "The cancer imaging archive (TCIA): Maintaining and operating a public information repository," *Journal of Digital Imaging*, vol. 26, no. 6, pp. 1045–1057, 2013, doi: 10.1007/s10278-013-9622-7.

[18] R. C. Gonzalez and R. E. Woods, *Digital Image Processing*, 4th ed. Upper Saddle River, 2018.

[19] X. Ren and S. Lai, "Medical Image Enhancement Based on Laplace Transform, Sobel Operator and Histogram Equalization,"

Academic Journal of Computing & Information Science, vol. 5, no. 6, pp. 48–54, Jul. 2022, doi: 10.25236/AJCIS.2022.050608.
[20] W. K. Pratt, *Digital Image Processing*.Wiley, Jun. 14, 2006. doi: 10.1002/0470097434.
[21] K. R. Castleman, *Digital Image Processing*, 2nd ed. USA: Prentice Hall: Upper Saddle River, 1996.
[22] B. Jähne, *Digital Image Processing*, 5th ed. Berlin/Heidelberg: Springer Berlin, Heidelberg, 2005.
[23] Z. Li, H. Jin, and X. Xing, "Edge detection algorithm of fractional order sobel operator for integer order differential filtering," *Comput. Eng. Appl*, vol. 54, pp. 179–184, 2018.
[24] S. M. Pizer *et al.*, "Adaptive Histogram Equalization and Its Variations.," *Computer vision, graphics, and image processing*, vol. 39, no. 3, pp. 355–368, 1987, doi: 10.1016/S0734-189X(87)80186-X.
[25] M. A. Al Wadud, M. H. Kabir, M. A. A. Dewan, and O. Chae, "A dynamic histogram equalization for image contrast enhancement," *IEEE Transactions on Consumer Electronics*, vol. 53, no. 2, pp. 593–600, 2007, doi: 10.1109/TCE.2007.381734.
[26] A. M. Reza, "Realization of the contrast limited adaptive histogram equalization (CLAHE) for real-time image enhancement," *Journal of VLSI Signal Processing Systems for Signal, Image, and Video Technology*, vol. 38, no. 1, pp. 35–44, 2004, doi: 10.1023/B:VLSI.0000028532.53893.82.
[27] K. He, X. Zhang, S. Ren, and J. Sun, "Delving deep into rectifiers: Surpassing human-level performance on imagenet classification," 2015, *IEEE*. doi: 10.1109/ICCV.2015.123.
[28] C. Dong, C. C. Loy, K. He, and X. Tang, "Image Super-Resolution Using Deep Convolutional Networks," *IEEE Transactions on Pattern Analysis and Machine Intelligence*, vol. 38, no. 2, pp. 295–307, 2016, doi: 10.1109/TPAMI.2015.2439281.
[29] B. Nirupama, B. S. Dhevdharsan, U. Shreya Reddy, J. Joshan Athanesious, and S. Kiruthika, "Diagnosis based image quality assessment and enhancement for low dose CT image," *Frontiers in Radiology*, vol. 5, 2025, doi: 10.3389/fradi.2025.1704113.
[30] S. S. Jui, Z. Guo, R. Jiang, J. Liu, and B. Li, "HybridFormer: a convolutional neural network-Transformer architecture for low dose computed tomography image denoising," *PeerJ Computer Science*, vol. 11, p. e2952, 2025, doi: 10.7717/peerj-cs.2952.

BIOGRAPHIES OF AUTHORS

Md. Mehedi Hasan received the B.S. degree in Pure Mathematics from the University of Dhaka, Dhaka-1000, Bangladesh, in 2020, and the Master's degree in Mathematics from the University of Dhaka, Dhaka-1000, Bangladesh, in 2021. He is currently a Lecturer in Mathematics, Department of General Education, University of Frontier Technology, Bangladesh. His current research interests include on mathematical biology, mathematical programming, different areas of operation research and optimization, stochastic optimization, and machine learning. He can be contacted at email: mehedi0001@uftb.ac.bd.

Sujon Chandra Sutradhar is currently serving as a Lecturer in Mathematics, Department of General Education at the University of Frontier Technology, Bangladesh. He is currently serving as the Chief Researcher on a UGC-funded project and is actively engaged in several collaborative research initiatives with fellow academics. His research interests include machine learning, deep learning, computer vision, financial mathematics, mathematical biology. He can be contacted at email: sujon0001@uftb.ac.bd.

Zannatul Ferdushie is a Lecturer in the Department of Educational Technology and Engineering at the University of Frontier Technology, Bangladesh. She holds a Bachelor of Education (Honours) degree in Education (2020) and a Master's degree in Special Education (2023), both from the Institute of Education and Research, University of Dhaka. Her research interests include educational technology, artificial intelligence in education, learning design, special and inclusive education, STEM and STEAM education, pedagogy, assessment, and evaluation. She can be contacted at email: zannatul0001@uftb.ac.bd.

Rabeya Basri is a Lecturer in Business Management at the Department of General Education at the University of Frontier Technology, Bangladesh. She holds a Bachelor of Business Administration (BBA) degree in Management (2020) and a Master's in Business Administration (MBA) degree in Strategic and International Management (SIM) (2023), both from Faculty of Business Studies, University of Dhaka. Her research interests include business strategy and leadership, entrepreneurship and innovation, business intelligence and management, supply chain management, human resource management, technology and digital transformation, project management, digital marketing, innovation and knowledge management, cross-cultural management, international trade policy, corporate strategy and competitive advantage, globalization and business transformation, cross cultural business ethics. She can be contacted at email: rabeya0001@uftb.ac.bd.